PHYSICAL REVIEW A **69**, 041801(R) (2004)

Generation of ultrabright tunable polarization entanglement without spatial, spectral, or temporal constraints

Marco Fiorentino,* Gaétan Messin, Christopher E. Kuklewicz, Franco N. C. Wong, and Jeffrey H. Shapiro
Research Laboratory of Electronics, Massachusetts Institute of Technology, Cambridge, Massachusetts 02139, USA
(Received 8 September 2003; published 5 April 2004)

The need for spatial and spectral filtering in the generation of polarization entanglement is eliminated by combining two coherently driven type-II spontaneous parametric down-converters. The resulting ultrabright source emits photon pairs that are polarization entangled over the entire spatial cone and spectrum of emission. We detect a flux of ~12 000 polarization-entangled pairs/s per mW of pump power at 90% quantum-interference visibility, and the source can be temperature tuned for 5 nm around frequency degeneracy. The output state is actively controlled by precisely adjusting the relative phase of the two coherent pumps.

DOI: 10.1103/PhysRevA.69.041801 PACS number(s): 42.65.Lm, 03.65.Ud, 03.67.Mn, 42.50.Dv

Polarization entanglement has been used to demonstrate a variety of quantum effects from quantum teleportation [1] to quantum cryptographic protocols [2]. The quality of polarization-entangled photon sources can be characterized by their pair flux and the purity of the entangled state they generate [3–7]. For the existing sources the requirements of high flux and high purity are often in conflict. Consider, for example, type-II spontaneous parametric down-conversion (SPDC) in a noncollinearly phase-matched β-barium borate (BBO) crystal. Here [4] spatial and spectral filtering are necessary to eliminate nonentangled photons that would reduce the purity of the output state. A source of polarization-entangled photons has been proposed [3] and demonstrated [6] in which the outputs of two different SPDC crystals are combined interferometrically. It was recognized that such a setup would generate entangled photons independent of their wavelengths and angles of emission [3]. The two-crystal interferometer, however, did not show the promised high flux and high visibilities [6]; this was attributed to technical difficulties in the alignment.

Our group has investigated the use of a collinearly propagating geometry and long periodically poled crystals to simplify alignment and to increase the output flux in both type-I [8] and type-II SPDC [9]. In the case of type-II SPDC in periodically poled potassium titanyl phosphate (PPKTP) [9], we have obtained *post selected* polarization-entangled photons. However, spatial and spectral filtering are still required to obtain a high-purity entangled state and the postselection process involves a 3-dB loss. In this Rapid Communication we report on a robust implementation of the coherent addition of two SPDC sources based on a single PPKTP crystal. Our scheme fully exploits, for the first time to our knowledge, the properties of interferometric combining of two coherent SPDC sources [3] to yield an ultrabright source of polarization entanglement that has no spatial or spectral constraints. Moreover, collinear operation allows us to control the output state by locking the pump phase of the same interferometer. This setup produces approximately ten times more polarization-entangled pairs/s per mW of pump than any other continuous-wave (cw) source in the literature [5,7].

Figure 1 illustrates a source that coherently combines the outputs of two SPDC crystals. A laser is split by a 50-50 beam splitter (BS) and pumps the two crystals that are phase matched for collinear type-II SPDC. In the low-gain regime, the biphoton state just after the crystals is given by

$$|\Psi\rangle = \frac{1}{\sqrt{2}}(|H_A(\omega_s)V_A(\omega_i)\rangle + e^{i\phi_p}|H_B(\omega_s)V_B(\omega_i)\rangle), \quad (1)$$

where A and B refer to the two arms of the interferometer, ω_s and ω_i are the signal and idler frequencies, respectively, and $\phi_p = k_p(L_B - L_A)$ is the difference of the delays accumulated by the pump (with wave vector k_p) in the paths L_A and L_B between the 50-50 BS and the crystals. A half-wave plate (HWP) is used to rotate the polarizations by 90° in arm B, so that the output state after the polarizing beam splitter (PBS) is

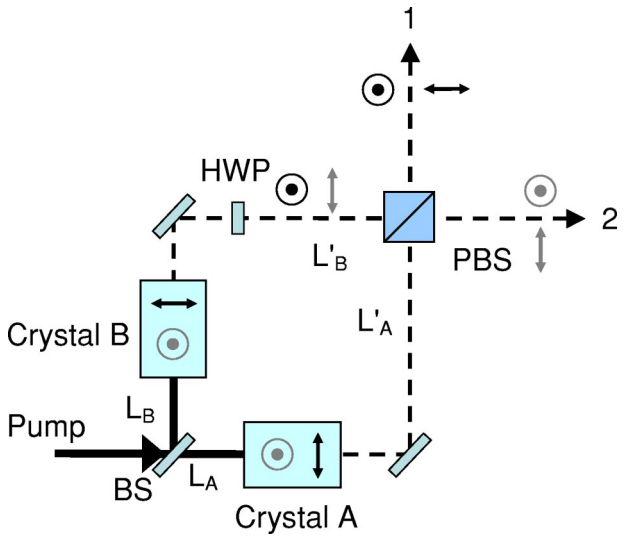

FIG. 1. Schematic of the two-crystal source of polarization-entangled photons. Black (gray) refers to the signal (idler) field amplitude at ω_s (ω_i). Horizontal (vertical) polarization: ↕ (⊙). BS, beam splitter; HWP, half-wave plate; PBS, polarizing beam splitter.

*Electronic address: mfiore@mit.edu

$$|\Psi\rangle = \frac{1}{\sqrt{2}}(|H_1(\omega_s)V_2(\omega_i)\rangle + e^{i\phi}|V_1(\omega_s)H_2(\omega_i)\rangle), \qquad (2)$$

where 1 and 2 refer to the two PBS output ports. The overall phase $\phi=\phi_p+\phi_s+\phi_i$ is determined by the pump phase ϕ_p and the phase delays accumulated by the signal and idler, respectively, with $\phi_{s,i}=k_{s,i}(L'_B-L'_A)-\Delta\phi_{\lambda/2}(\omega_{s,i})$. The first term of $\phi_{s,i}$ is the delay due to the arm lengths L'_A and L'_B between the crystals and the PBS, and the second term is the phase difference introduced by the HWP. Note that the phase delays introduced by the identical crystals in the two arms cancel. Under collinear phase matching $k_p=k_s+k_i$, and ϕ is equal to the phase difference accumulated by the pump in the Mach-Zehnder interferometer formed between the 50-50 BS and the PBS except for a fixed offset due to the HWP. The phase of the output biphoton state in Eq. (2) can therefore be precisely controlled by locking the Mach-Zehnder interferometer as seen by the pump alone: one can generate the triplet (for $\phi=0$) or the singlet state ($\phi=\pi$), as well as intermediate states that are linear combinations thereof.

The HWP constrains the signal (idler) fields from the two crystals to exit at output 1 (2) in Fig. 1, ensuring [3,10] that the two sources are indistinguishable so that all the photons are polarization entangled regardless of their wavelengths and directions of emission. Spatial and spectral filtering is unnecessary in this two-crystal configuration, thus promising a source that has a much higher photon-pair flux, plus a larger bandwidth and spatial extension than BBO sources. Due to energy and momentum conservation, one expects the emitted photon pairs from this broadband spatially extended source to show spectral and spatial entanglement. Additional advantages of this scheme include automatic erasure of timing distinguishability, nondegenerate operation, and source tunability.

To implement the interferometric source described above it is crucial that the two SPDC sources be identical. Source differences introduce an element of distinguishability between the two paths that would lead to a mixed state output. We therefore implemented the scheme based on a single crystal with counterpropagating pump beams derived from a single laser. The single-crystal approach is particularly useful with periodically poled crystals, as it mitigates imperfections in the profiles of the periodic gratings.

We used a 10-mm-long (X crystallographic axis), 1-mm-thick (Z axis), and 4-mm-wide (Y axis) hydrothermally grown PPKTP crystal with a grating period of 9.0 μm. At a temperature of $\simeq$32 °C this grating period phase matches type-II collinear frequency-degenerate down-conversion of a 398.5-nm pump polarized along the Y axis and propagating along the crystal's X axis. The crystal was housed in an oven and was maintained at its operating temperature with ±0.1 °C precision. This crystal was previously characterized and used in type-II collinear SPDC to yield single-beam quantum interference with a 99% visibility [9]. We used second-harmonic generation to measure the temperature and wavelength tuning behavior in PPKTP using a cw tunable laser centered around 797 nm. The second-harmonic measurements are well described by the Sellmeier phase-matching equations for PPKTP [11], which allow us to calculate the spatial and spectral properties of the down-converted photons, as well as the phase-matching angles' dependence on the crystal temperature. The latter predictions have been verified by imaging the emitted photons with a charge-coupled-device camera and narrow spectral filters.

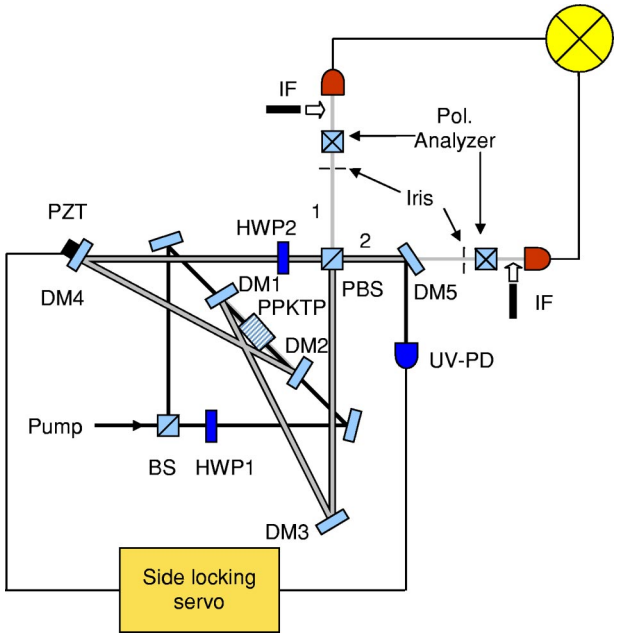

FIG. 2. Experimental setup. BS, 50-50 beam splitter; DM, dichroic mirror; PBS, polarizing beam splitter; HWP, half-wave plate; IF, 3-nm interference filter centered at 797 nm. HWP1 is used to balance the flux of down-converted photons in the two directions.

The experimental setup is shown in Fig. 2. The frequency-doubled cw Ti:sapphire pump laser at 398.5 nm was split by a BS that had a splitting ratio of ~50-50. To balance the powers of the two pump beams we inserted a half-wave plate (HWP1) to vary the horizontally polarized pump power in the (counterclockwise propagating) brighter path. The crystal was not phase matched for a vertically polarized pump. Each pump beam focused to a waist of ~150 μm at the center of the PPKTP crystal. The generated beams were collimated with 300-mm radius-of-curvature dichroic mirrors (DM1,2) and combined at a PBS after the polarization of one of the beams was rotated by 90° with a HWP. The dichroic mirrors were coated for high reflectivity (HR) at 797 nm and for high transmission (HT) at 398.5 nm, with a residual reflectivity of 0.2% at the pump wavelength. The pump beams, which propagated collinearly with the down-converted beams, were weakly reflected by the four mirrors (DM1-4) and recombined on the PBS, which had a ~20-80 splitting ratio at the pump wavelength. The resultant pump beam from port 2 of the PBS was directed by a dichroic mirror (DM5, HR at 398.5 nm, and HT at 797 nm) for detection with an ultraviolet photodiode. The BS and PBS in Fig. 2 formed a Mach-Zehnder interferometer for the pump and the detected fringes were used to stabilize the interferometer with a side-locking technique. This provided a convenient and robust way to control the phase ϕ of the output state in Eq. (2). By inserting a dispersive medium (such as a thin glass plate) in one of the arms of the Mach-Zehnder interferometer we introduced

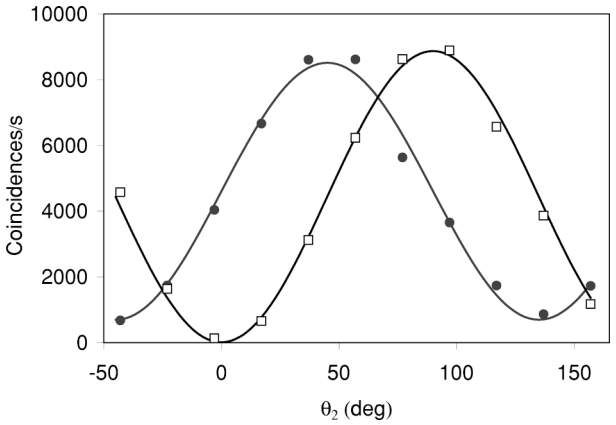

FIG. 3. Coincidence counts for the frequency-degenerate singlet state versus analyzer angle θ_2 in arm 2 for analyzer angle in arm 1 set at 45° (solid circles) and 0° (open squares). Aperture size: 4 mm; no interference filter was used; pump power: 0.7 mW. Each point is averaged over 10 s and the lines are a sinusoidal fit to the data.

a fixed but variable offset between the phase of the pump fringes and the phase of the output state (the overall offset phase includes other dispersive elements in the interferometer). By varying this phase offset, we were able to lock the phase of the output state at an arbitrary value while optimizing the side-locking feedback signal.

We placed two irises in the output beam paths to control the acceptance angle of the detection system. We estimate that an iris diameter of 1 mm corresponded to an internal emission solid angle of $\sim 3.5\times10^{-5}$ sr at the crystal. Flat dichroic mirrors (not shown in Fig. 2) similar to DM1 were used to eliminate residual pump light. The output photons were detected with single-photon Si detectors (Perkin-Elmer SPCM-AQR-14) through polarization analyzers (composed of a half-wave plate and a polarizer). The outputs of the single-photon detectors were counted and also sent to an AND gate (TTL logic family 74F) for coincidence counting. The coincidence window for this configuration was measured to be 39.4 ns. This parameter allowed us to correct for the rate of accidental coincidences in all of the data reported. For example, when 12 000 coincidences/s were measured, an average of 67 000 singles/s were detected at each single-photon detector and ~250 coincidences/s were due to accidental Poisson processes (better coincidence logic would make this correction unnecessary).

A summary of our experimental results, with the accidentals removed, is shown in Figs. 3–5 for $\phi=\pi$ (singlet). The temperature of the crystal was set to ~32 °C to ensure frequency degenerate operation. Figure 3 shows the quantum interference in the coincidence counts when the analyzer angle in arm 2 was varied for a fixed angle in arm 1 with no narrow-band interference filter. We observed a visibility of $(100\pm3)\%$ $[(85\pm3)\%]$ when analyzer 1 is set to 0° (45°). In what follows we will use the 45° visibility as an indication of the quality of the state generated.

In Fig. 4 we report the 45° visibility for the singlet state as a function of the iris diameter. Two sets of data are shown, one using a 3-nm interference filters centered at 797 nm

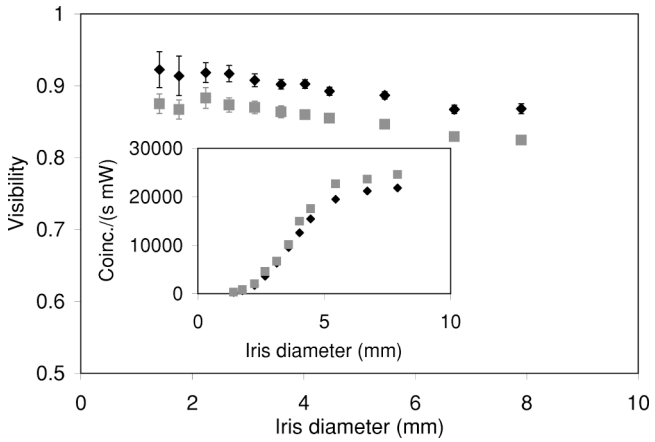

FIG. 4. Frequency-degenerate singlet state 45°-visibility versus iris diameter. In the inset: coincidence counts/s per mW of pump power versus iris diameter. No interference filter (squares) and 3-nm interference filter centered at 797 nm (diamonds).

placed in front of the detectors (diamonds) and one in which the interference filter was removed (squares). In both cases the visibility is almost constant as a function of the iris diameter. This allows us to increase the pair flux (Fig. 4 inset) while preserving the purity of the output state. With the 3-nm filter we observed a visibility of 90% and a flux $\simeq$12 000 pairs s^{-1} mW^{-1} with a 4-mm iris. Under this condition, following Ref. [12], we tested Bell's inequality and obtained $S=2.599\pm0.004$, violating the classical limit by more than 100σ.

Figure 4 can be compared with data obtained in a single-pass configuration with similar collection geometry properties reported in Ref. [9]. The visibility of quantum interference in the single-pass experiment drops much faster as the iris diameter increases than in this interferometric configuration. The nearly constant visibility in Fig. 4 arises from effective spatial and spectral indistinguishability in this dual-pumped interferometric configuration.

Two main factors limited the visibility: wave-front distortion and diffraction caused by the components of the inter-

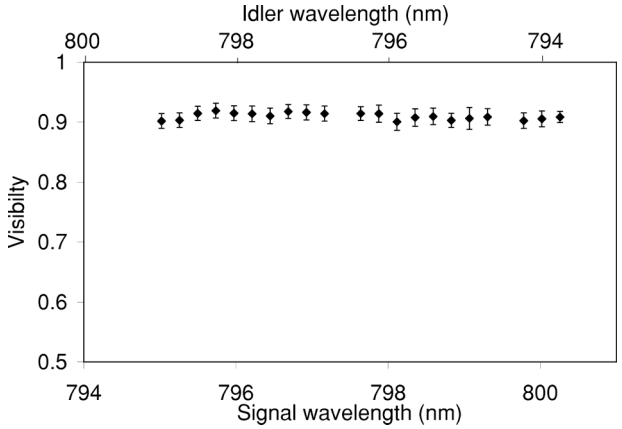

FIG. 5. 45° visibility (corrected for accidentals) versus signal wavelength (no interference filter, iris diameter 2.2 mm) with a measured flux of 3500 pairs s^{-1} mW^{-1}. The wavelengths on the abscissas are calculated from temperature tuning curves of the Sellmeier equations.

ferometer, and defects in the electric-field poling of the crystal. Wave-front distortion and diffraction lead to spatial distinguishability between the two down-converted beams. Inhomogeneity in the crystal grating introduces a temporal mismatch between the two paths. Both these effects were mitigated somewhat by closing the iris and by adding spectral filters. To investigate the effects of wave-front distortion and diffraction we measured the interferometer visibility directly by injecting a laser beam at 797 nm through arm 2 of the PBS in Fig. 2 and observing the fringe signal in arm 1. The input and output beam diameters could be varied with irises. When we changed the diameter of the output beam for a fixed input beam diameter, the visibility showed the same plateau for small iris diameters as in Fig. 4. When we decreased the input beam diameter for a fixed output beam diameter the visibility increased linearly, approaching 100%. This suggests that the diffraction inside the interferometer was responsible for the flat plateau in the visibility of Fig. 4. We note that a slight mismatch in the length of the two interferometric arms can also degrade the visibility.

No interference filter was used in obtaining the data shown in Fig. 5 and the iris diameter was fixed at 2.2 mm. The temperature of the crystal was then scanned between 20 °C and 50 °C and the 45° visibility was measured. We used our knowledge of the Sellmeier equations, verified by down-conversion and second-harmonic generation measurements, to calculate the phase-matched signal and idler wavelengths for each temperature setting, and hence obtain the abscissas shown in this figure. Figure 5 shows that the 45° visibility is essentially independent of the signal and idler emission wavelengths for a range of ~5 nm around degeneracy.

In conclusion, we have demonstrated a source of polarization-entangled photon pairs with high flux and state purity. The cw source is based on the interferometric combination of two coherently driven type-II sources of spontaneous parametric down-conversion from a single PPKTP crystal. This dual-pumped source is uniquely characterized by the fact that all the emitted photon pairs are polarization entangled, regardless of their wavelengths and directions of emission. Therefore it can be tuned, has a wide bandwidth, and an extended spatial profile. We believe that our source produces spatial and spectral entanglement, in addition to polarization entanglement, thus providing additional degrees of freedom that can be used for quantum communication. Further work with this source is needed to experimentally demonstrate these additional forms of entanglement. If successful, we would then have a source that could be used to demonstrate fundamental quantum properties [13] and in cryptographic protocols with improved security [14].

This work was supported by a DoD Multidisciplinary University Research Initiative (MURI) program administered by the Army Research Office under Grant No. DAAD-19-00-1-0177, the Defense Advanced Research Projects Agency (DARPA) and Air Force Research Laboratory under Grant No. F30602-01-2-0546, the National Reconnaissance Office, and a DURIP Instrumentation Grant No. DAAD-19-01-1-0335.

[1] D. Bouwmeester *et al.*, Nature (London) **390**, 575 (1997).

[2] T. Jennewein, C. Simon, G. Weihs, H. Weinfurter, and A. Zeilinger, Phys. Rev. Lett. **84**, 4729 (2000); D. S. Naik, C. G. Peterson, A. G. White, A. J. Berglund, and P. G. Kwiat, *ibid.* **84**, 4733 (2000).

[3] P. G. Kwiat, P. H. Eberhard, A. M. Steinberg, and R. Y. Chiao, Phys. Rev. A **49**, 3209 (1994).

[4] P. G. Kwiat *et al.*, Phys. Rev. Lett. **75**, 4337 (1995).

[5] P. G. Kwiat, E. Waks, A. G. White, I. Appelbaum, and P. H. Eberhard, Phys. Rev. A **60**, R773 (1999).

[6] Y. H. Kim, M. V. Chekhova, S. P. Kulik, M. H. Rubin, and Y. Shih, Phys. Rev. A **63**, 062301 (2001).

[7] C. Kurtsiefer, M. Oberparleiter, and H. Weinfurter, Phys. Rev. A **64**, 023802 (2001); J. Völtz, C. Kurtsiefer, and H. Weinfurter, Appl. Phys. Lett. **79**, 869 (2001); M. Barbieri, F. De Martini, G. Di Nepi, and P. Mataloni, e-print quant-ph/0303018; M. Pelton *et al.* (unpublished).

[8] E. J. Mason, M. A. Albota, F. König, and F. N. C. Wong, Opt. Lett. **27**, 2115 (2002).

[9] C. E. Kuklewicz, M. Fiorentino, G. Messin, F. N. C. Wong, and J. H. Shapiro, Phys. Rev. A **69**, 013807 (2004).

[10] J. H. Shapiro and N. C. Wong, J. Opt. B: Quantum Semiclassical Opt. **2**, L1 (2000).

[11] H. Vaherzeele, J. D. Bierlein, and F. C. Zumsteg, Appl. Opt. **27**, 3314 (1988); W. Wiechmann, S. Kubota, T. Fukui, and H. Masuda, Opt. Lett. **18**, 1208 (1993).

[12] J. F. Clauser, M. A. Horne, A. Shimony, and R. A. Holt, Phys. Rev. Lett. **23**, 880 (1969); A. Aspect, P. Grangier, and G. Roger, *ibid.* **49**, 91 (1982).

[13] Z.-B. Chen, J.-W. Pan, Y.-D. Zhang, C. Brukner, and A. Zeilinger, Phys. Rev. Lett. **90**, 160408 (2003).

[14] M. Genovese and C. Novero, Eur. Phys. J. D **21**, 109 (2002).